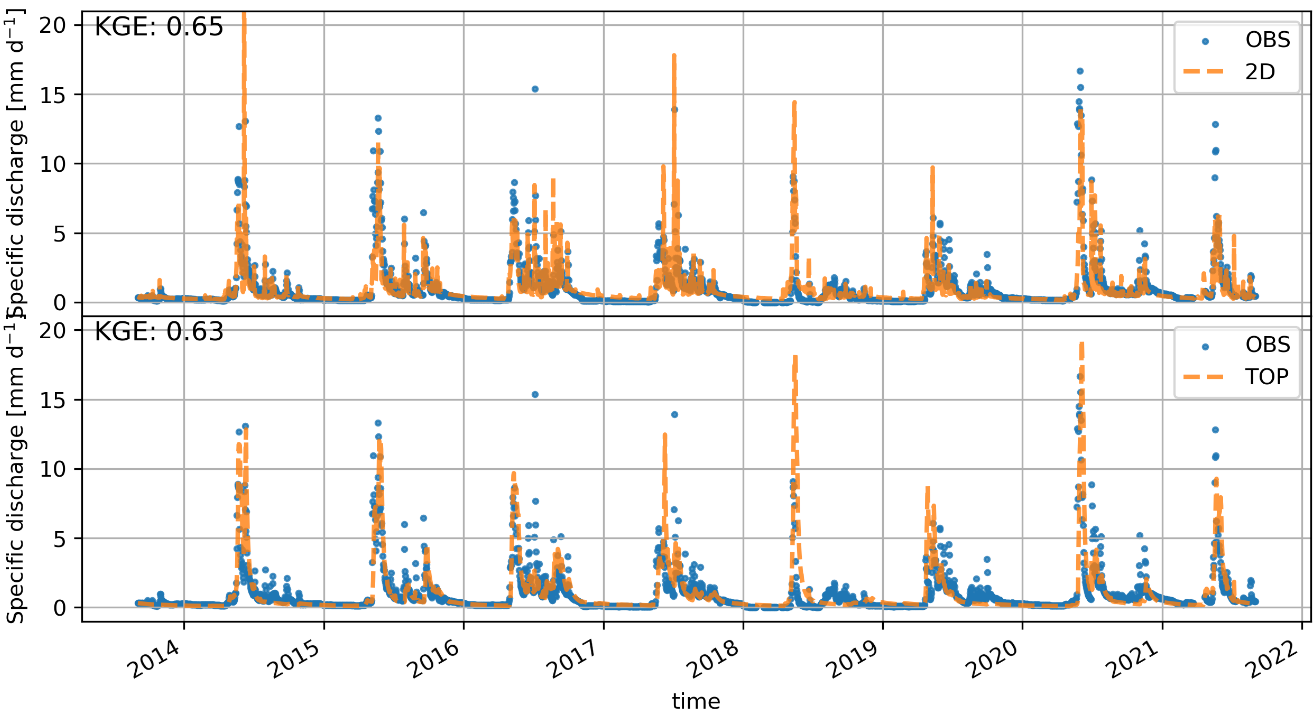


**Figure S1.** Comparison of specific discharges simulated by 2D (upper row) and TOP (lower row) conceptualizations against observations. Some observations are missing between April and June in 2018. KGE refers to the Kling-Gupta Efficiency (Gupta et al., 2009).

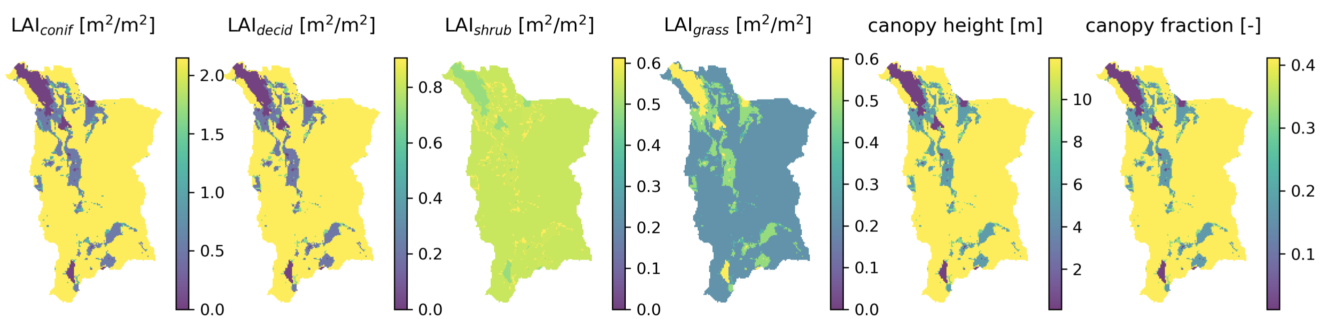


**Figure S2.** Site averaged vegetation GIS rasters.

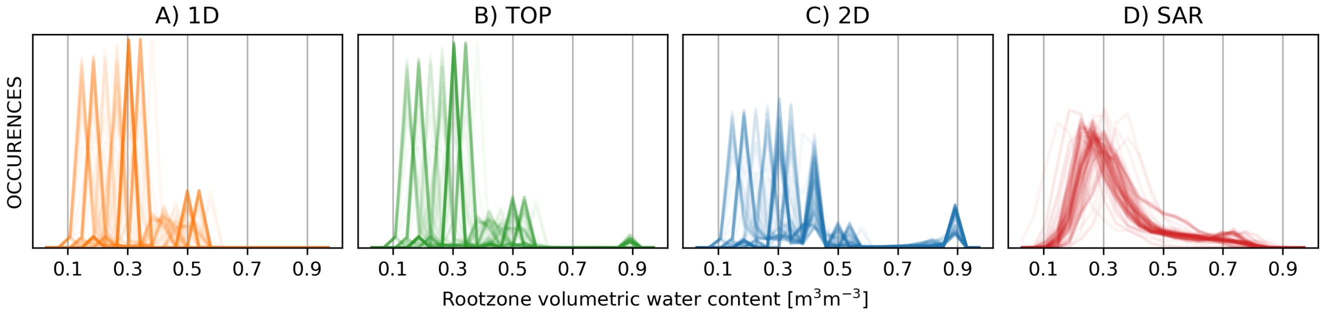


**Figure S3.** Daily distributions of simulated rootzone soil moisture (1D, TOP and 2D) and SAR-based surface soil moisture.

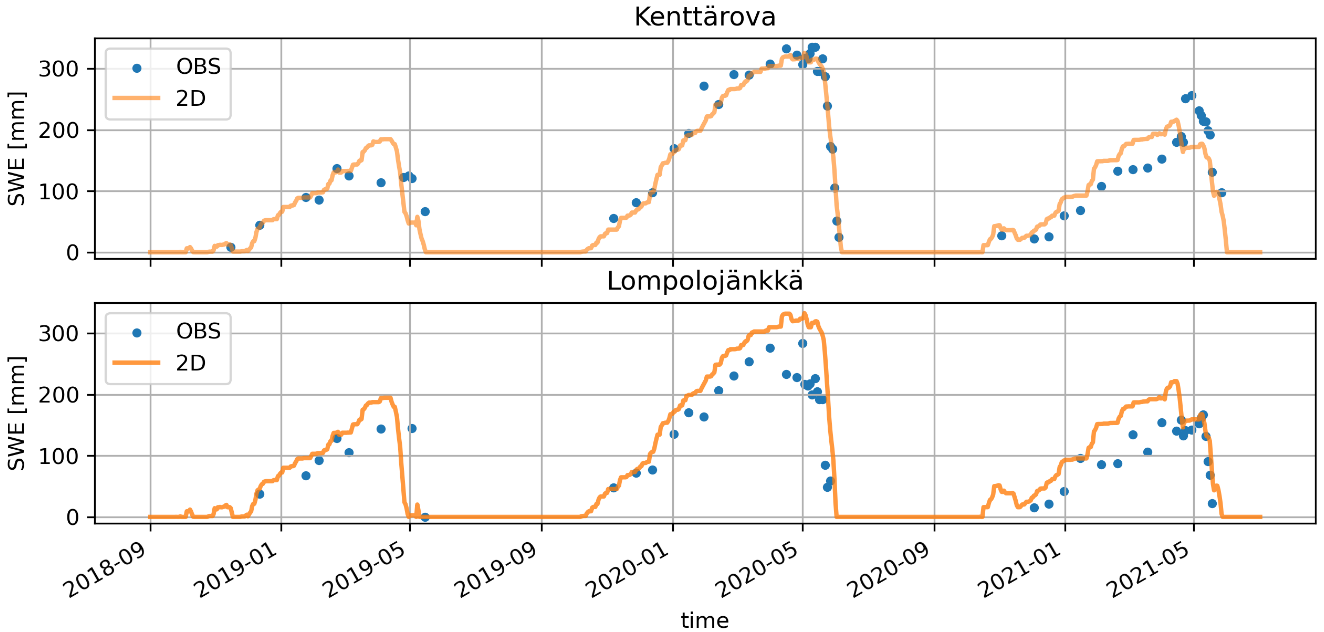


**Figure S4.** Comparison of simulated and observed snow water equivalent (SWE) from 2018 autumn to 2021 summer at Kenttärova and Lompolojänkkä sites.

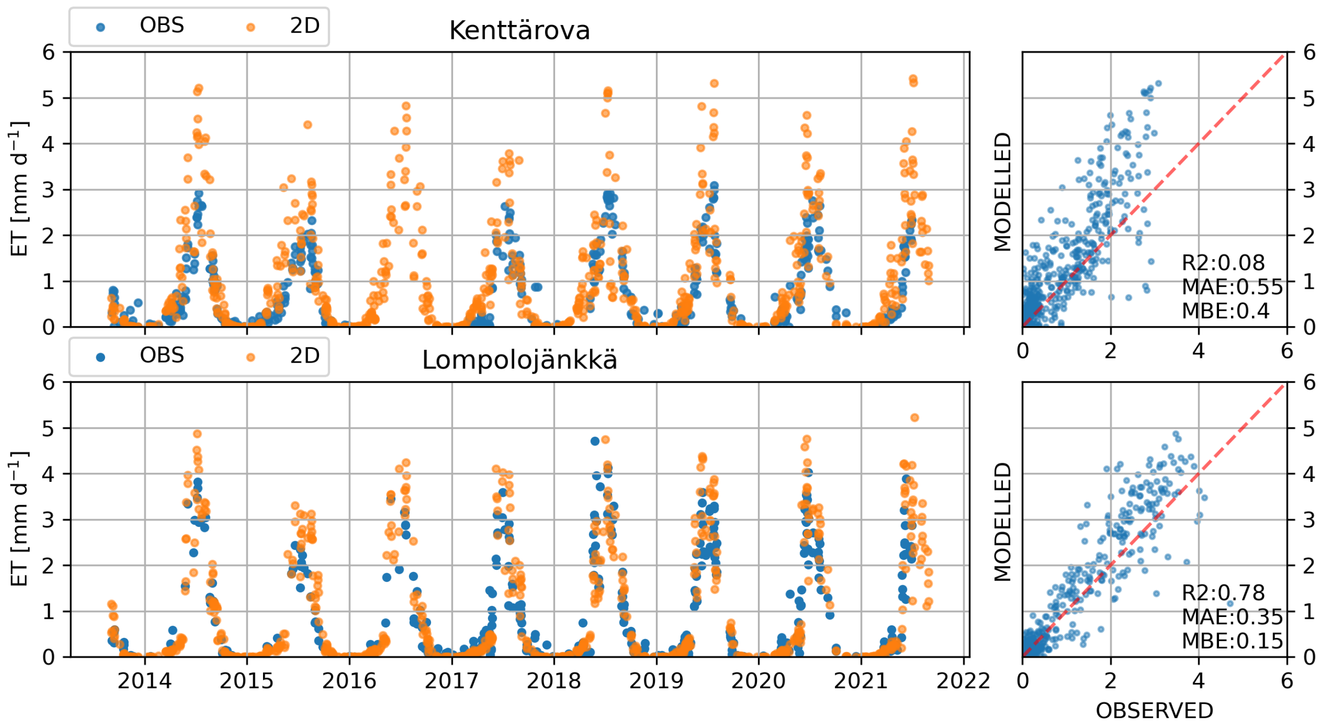


**Figure S5.** Comparison of simulated and observed evapotranspiration (ET) at Kenttärova and Lompolojänkkä sites. Only dry-canopy conditions (i.e. no precipitation during the current or previous day), and days with more than 90 % available hourly ET observations were considered.

**Table 1.** Site type -specific organic moss-humus layer hydraulic parameters. The $\theta_{s,org}$, $\theta_{fc,org}$ and $\theta_{wp,org}$ are porosity, field capacity and wilting point, respectively. $K_{sat,org}$ is saturated hydraulic conductivity and $\beta_{org}$ is a parameter describing power-law decay of hydraulic conductivity with decreasing saturation ratio.

| Site | $\theta_{s,org}$ ($m^3$ $m^{-3}$) | $\theta_{fc,org}$ ($m^3$ $m^{-3}$) | $\theta_{wp,org}$ ($m^3$ $m^{-3}$) | $K_{sat,org}$ (m $s^{-1}$) | $\beta_{org}$ (-) | Source |
|---|---|---|---|---|---|---|
| Mineral | 0.90 | 0.30 | 0.20 | $1 \cdot 10^{-3}$ | 6.0 | Williams and Flanagan (1996); Elumeeva et al. (2011) |
| Spruce mire | 0.90 | 0.65 | 0.30 | $1 \cdot 10^{-3}$ | 6.0 | Williams and Flanagan (1996); Elumeeva et al. (2011) |
| Pine mire | 0.90 | 0.65 | 0.30 | $1 \cdot 10^{-3}$ | 6.0 | Williams and Flanagan (1996); Elumeeva et al. (2011) |
| Treeless mire | 0.90 | 0.65 | 0.30 | $1 \cdot 10^{-3}$ | 6.0 | Williams and Flanagan (1996); Elumeeva et al. (2011) |

**Table 2.** Soil type -specific rootzone layer hydraulic parameters. The $\theta_{s,root}$, $\theta_{fc,root}$ and $\theta_{wp,root}$ are porosity, field capacity and wilting point, respectively. $K_{sat,root}$ is saturated hydraulic conductivity and $\beta_{root}$ is a parameter describing power-law decay of hydraulic conductivity with decreasing saturation ratio.

| Soil texture | $\theta_{s,root}$ ($m^3$ $m^{-3}$) | $\theta_{fc,root}$ ($m^3$ $m^{-3}$) | $\theta_{wp,root}$ ($m^3$ $m^{-3}$) | $K_{sat,root}$ (m $s^{-1}$) | $\beta_{root}$ (-) | Source |
|---|---|---|---|---|---|---|
| Coarse | 0.41 | 0.21 | 0.10 | $1 \cdot 10^{-4}$ | 3.1 | Launiainen et al. (2019) |
| Medium | 0.43 | 0.33 | 0.13 | $1 \cdot 10^{-5}$ | 4.7 | Launiainen et al. (2019) |
| Peat | 0.89 | 0.53 | 0.36 | $3 \cdot 10^{-4}$ | 6.0 | Autio et al. (2023) |

**Table 3.** Soil type -specific deep layer parameters. The $\theta_{s,deep}$ and $\theta_{r,deep}$ are porosity and residual water content parameter, respectively. The $\alpha$ and $n$ are van Genuchten-Mualem fitting parameters (van Genuchten, 1980). The $K_{sat,root}$ is saturated hydraulic conductivity.

| Soil texture | $\theta_{s,deep}$ ($m^3$ $m^{-3}$) | $\theta_{r,deep}$ ($m^3$ $m^{-3}$) | $\alpha$ (-) | $n$ (-) | $K_{sat,deep}$ (m $s^{-1}$) | Source |
|---|---|---|---|---|---|---|
| Coarse | 0.41 | 0.05 | 0.024 | 1.20 | $1 \cdot 10^{-5}$ | Launiainen et al. (2019) |
| Medium | 0.43 | 0.05 | 0.024 | 1.20 | $1 \cdot 10^{-5}$ | Launiainen et al. (2019) |
| Peat | 0.89 | 0.20 | 0.072 | 1.26 | $1 \cdot 10^{-5}$ | Autio et al. (2023) |

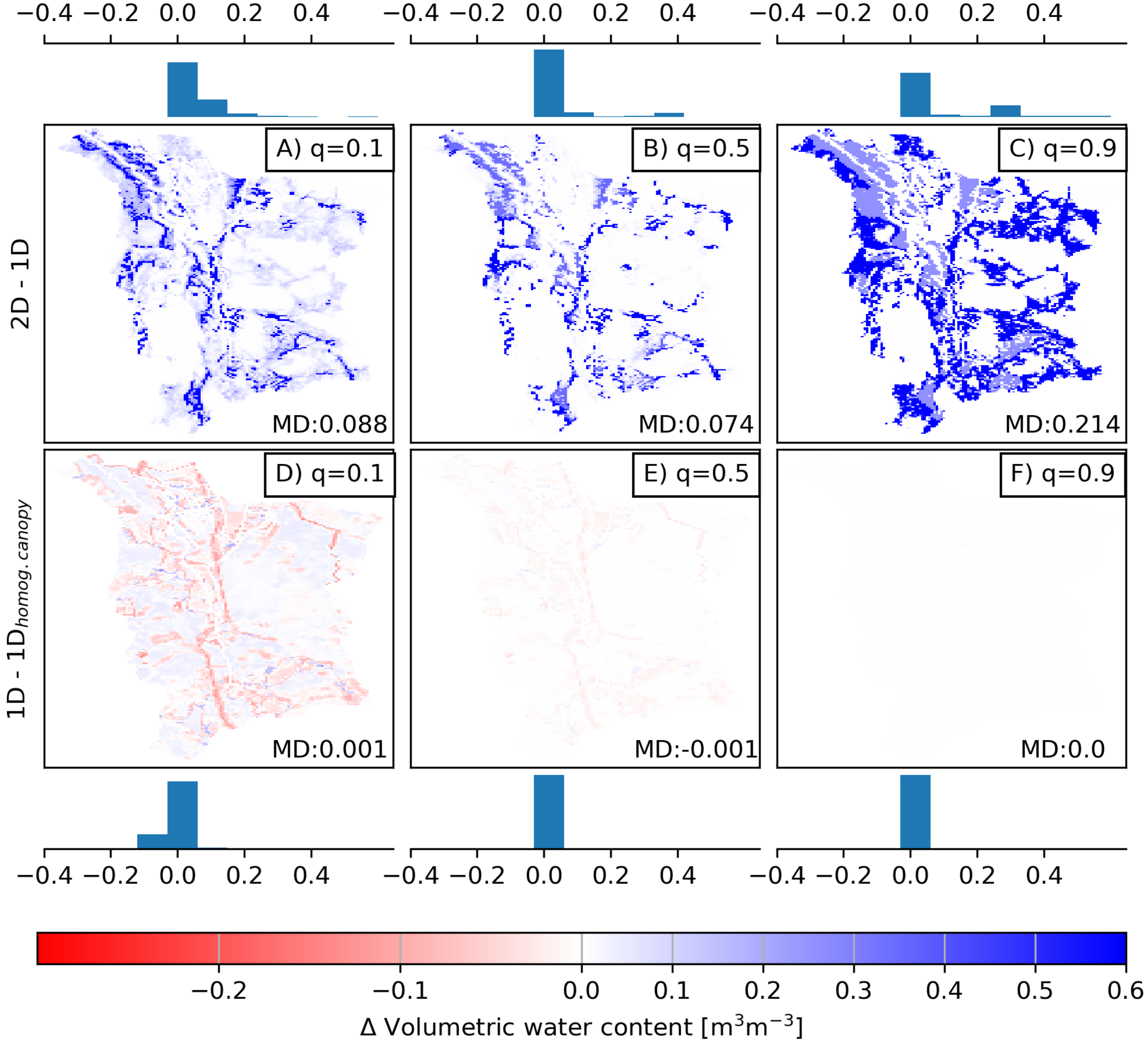


**Figure S6.** The impact of lateral groundwater flow (upper row) on organic moss-humus layer soil moisture expressed as Δ = 2D - 1D, and the impact of vegetation heterogeneity (bottom row) expressed as Δ = 1D - 1D$_{homog.canopy}$ in different catchment soil moisture states. The panels correspond to 0.1, 0.5, and 0.9 quantiles of grid-cell soil moisture, and the bars show distribution of binned differences. Mean difference (MD) is shown in each panel.

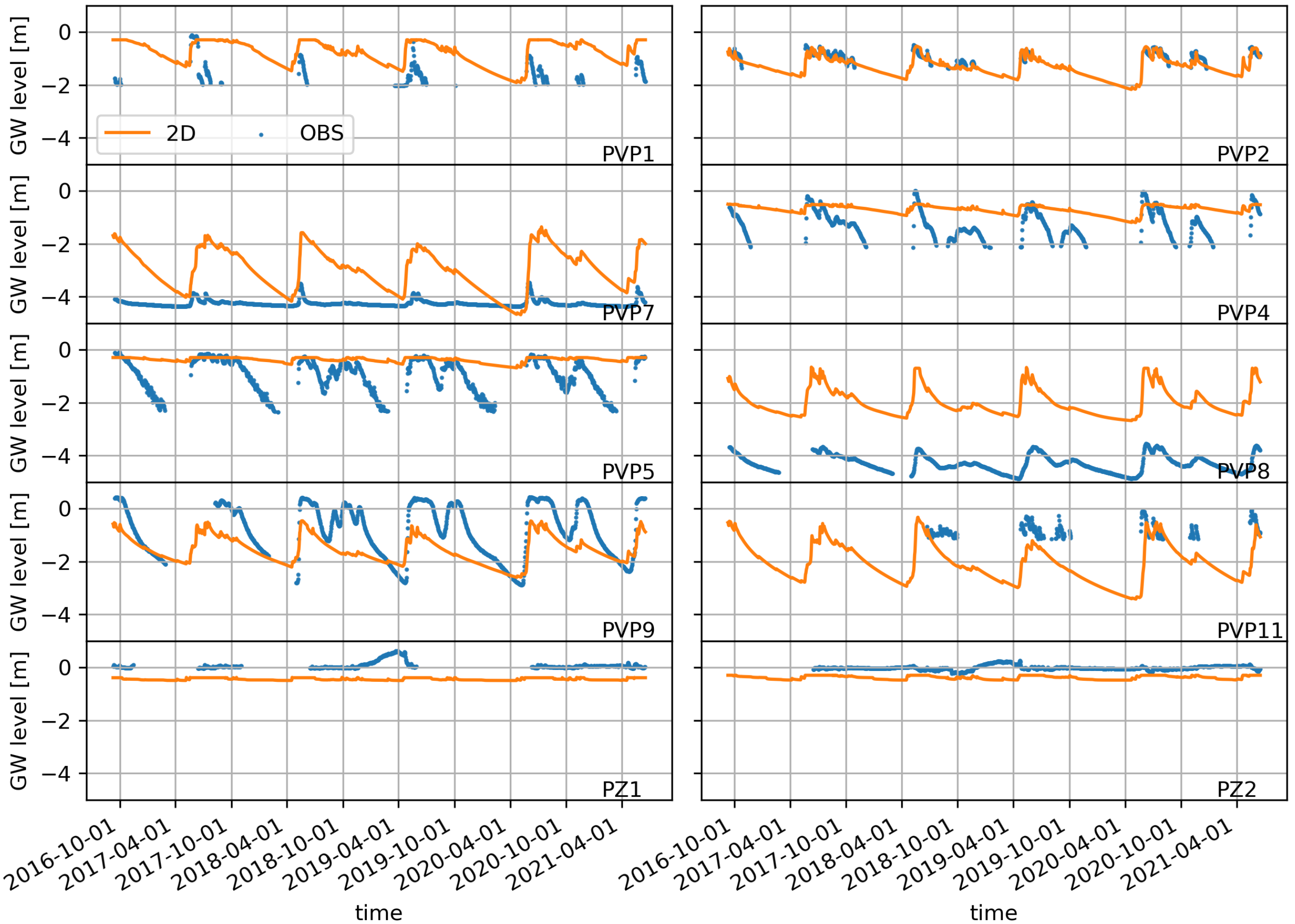


**Figure S7.** Temporal dynamics of 2D simulated and in-situ measured groundwater levels at 10 different locations around the catchment.

## References


Autio, A., Ala-Aho, P., Rossi, P. M., Ronkanen, A.-K., Aurela, M., Lohila, A., Korpelainen, P., Kumpula, T., Klöve, B., and Marttila, H.: Groundwater exfiltration pattern determination in the sub-arctic catchment using thermal imaging, stable water isotopes and fully-integrated groundwater-surface water modelling, Journal of Hydrology, 626, 130 342, https://doi.org/https://doi.org/10.1016/j.jhydrol.2023.130342, 2023.

Elumeeva, T. G., Soudzilovskaia, N. A., During, H. J., and Cornelissen, J. H.: The importance of colony structure versus shoot morphology for the water balance of 22 subarctic bryophyte species, Journal of Vegetation Science, 22, 152–164, https://doi.org/10.1111/j.1654-1103.2010.01237.x, 2011.

Gupta, H. V., Kling, H., Yilmaz, K. K., and Martinez, G. F.: Decomposition of the mean squared error and NSE performance criteria: Implications for improving hydrological modelling, Journal of Hydrology, 377, 80–91, https://doi.org/https://doi.org/10.1016/j.jhydrol.2009.08.003, 2009.

Launiainen, S., Guan, M., Salmivaara, A., and Kieloaho, A. J.: Modeling boreal forest evapotranspiration and water balance at stand and catchment scales: a spatial approach, Hydrology and Earth System Sciences, 23, 3457–3480, https://doi.org/10.5194/hess-23-3457-2019, 2019.

van Genuchten, M. T.: A Closed-form Equation for Predicting the Hydraulic Conductivity of Unsaturated Soils, Soil Science Society of America Journal, 44, 892–898, https://doi.org/10.2136/sssaj1980.03615995004400050002x, 1980.

Williams, T. G. and Flanagan, L. B.: Effect of changes in water content on photosynthesis, transpiration and discrimination against 13CO2 and C18O16O in Pleurozium and Sphagnum, Oecologia, 108, 38–46, https://doi.org/10.1007/BF00333212, 1996.